(12)

DNA 3282T

A RADIATION DIFFUSION AND HYDRODYNAMICS CODE FOR LOW-ALTITUDE MULTIPLE BURSTS

Mission Research Corporation
735 State Street
Santa Barbara, California 93101

15 July 1975

Topical Report for Period 1 April 1972—30 September 1973

CONTRACT No. DNA 001-75-C-0142

APPROVED FOR PUBLIC RELEASE;
DISTRIBUTION UNLIMITED.

THIS WORK SPONSORED BY THE DEFENSE NUCLEAR AGENCY
UNDER SUBTASK S99QAXHC061-78.

Prepared for
Director
DEFENSE NUCLEAR AGENCY
Washington, D. C. 20305

Destroy this report when it is no longer needed. Do not return to sender.

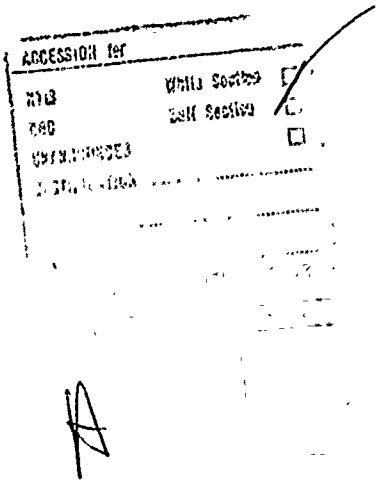

UNCLASSIFIED

SECURITY CLASSIFICATION OF THIS PAGE (When Data Entered)

(12) 38 P.

(19) REPORT DOCUMENTATION PAGE

READ INSTRUCTIONS BEFORE COMPLETING FORM

(18) 1. REPORT NUMBER: DNA 3282T

2. GOVT ACCESSION NO.

3. RECIPIENT'S CATALOG NUMBER (9)

(6) 4. TITLE (and Subtitle): A RADIATION DIFFUSION AND HYDRODYNAMICS CODE FOR LOW-ALTITUDE MULTIPLE BURSTS.

5. TYPE OF REPORT & PERIOD COVERED: Topical Report for Period 1 Apr 72—30 Sep 73

6. PERFORMING ORG. REPORT NUMBER: MRC-R-77

(14)

(10) 7. AUTHOR(s): Robert E. Stoeckly

(15) 8. CONTRACT OR GRANT NUMBER(s): DNA 001-75-C-0142

9. PERFORMING ORGANIZATION NAME AND ADDRESS: Mission Research Corporation, 735 State Street, Santa Barbara, California 93101

(16) DNA

10. PROGRAM ELEMENT, PROJECT, TASK AREA & WORK UNIT NUMBERS: NWED-Subtask S99QAXHC061-78

11. CONTROLLING OFFICE NAME AND ADDRESS: Director, Defense Nuclear Agency, Washington, D. C. 20305

(17) C061

(11)

12. REPORT DATE: 15 July 1975

13. NUMBER OF PAGES: 40

14. MONITORING AGENCY NAME & ADDRESS (if different from Controlling Office)

15. SECURITY CLASS. (of this report): UNCLASSIFIED

15a. DECLASSIFICATION/DOWNGRADING SCHEDULE

16. DISTRIBUTION STATEMENT (of this Report)

Approved for public release; distribution unlimited.

17. DISTRIBUTION STATEMENT (of the abstract entered in Block 20, if different from Report)

18. SUPPLEMENTARY NOTES

This work sponsored by the Defense Nuclear Agency under Subtask S99QAXHC061-78.

19. KEY WORDS (Continue on reverse side if necessary and identify by block number)

Low-altitude Nuclear Bursts
Multiple Bursts
Radiation Diffusion in Fireballs
X-Ray Deposition

20. ABSTRACT (Continue on reverse side if necessary and identify by block number)

This paper describes a computer code for studying strongly interacting multiple air bursts at low altitude. It is designed to study both early and late phases of two (or more) nonsimultaneous bursts at different positions along a vertical line. → cont on p 1473 B

DD FORM 1 JAN 73 1473 EDITION OF 1 NOV 65 IS OBSOLETE

UNCLASSIFIED

SECURITY CLASSIFICATION OF THIS PAGE (When Data Entered)

406 548

20. ABSTRACT (Continued)

The code is a two-dimensional modification of the one-fluid, implicit, Eulerian hydrodynamic code MICE. The modification described here treats radiative energy transfer in the approximation of radiation diffusion (or local thermodynamic equilibrium). This modification also treats in a rudimentary way the loss of thermal radiation from fireballs: this is calculated by using Planck mean opacities for one frequency interval ($0 < h\nu < 4.18$ ev) to integrate the optical depth from each cell to infinity in several directions. These treatments complement one another in the sense that the radiation diffusion transfers radiant energy during a time step from each cell to the immediately adjacent cells, while the radiation loss term transfers radiant energy from each cell to infinity. The difference equations involve (further) use of the technique of time-step splitting and are implicit. The relations used for the equations of state and the Rosseland and Planck mean opacities of air are plotted, and the method for initial X-ray deposition is described. To get satisfactory results, the radiation loss rate has been artifically increased to force the correct total radiation loss.

PREFACE

The author is indebted to F. E. Fajen, D. H. Sowle, and P. G. Fischer for discussions of this work.

TABLE OF CONTENTS

I INTRODUCTION

One of the major problems with phenomenology codes for nuclear explosions is our lack of understanding of the interaction between multiple bursts. To study multiple bursts in which two fireballs interact requires a two-dimensional radiation-hydrodynamics code for the radiative phase; in addition, it is most helpful if the later hydrodynamics can be studied by the same code, rather than by transferring back and forth between two codes. Several such efforts are now in progress. Extending the MICE hydrodynamic code to treat radiation is an attractive method: in addition to the advantage of a single code for early and late times, distinctive features of this code make it both fast (because the difference equations are implicit) and flexible and simple to use (because of the technique of time-step splitting). Recognizing this, the Defense Nuclear Agency authorized Mission Research Corporation to extend this code to treat radiation diffusion.

The basic MICE hydrodynamic code is described in Ref. 1. It is a one-fluid, Eulerian code that works in any of several geometries. The treatment of magnetic fields in the basic code has been dropped in this version, which is intended only for low altitudes. This version treats radiative energy transfer in the approximation of radiation diffusion (or local thermodynamic equilibrium) - that is, in the approximation that the photon mean free path is small compared to distances over which the temperature changes appreciably. This approximation is sufficient for early times for bursts below 40 km altitude. The treatment of radiation currently assumes symmetry about the vertical axis and uses two-dimensional cylindrical (or one-dimensional spherical) coordinates.

Section II presents the physical equations, including initial conditions and boundary conditions and the equations of state and opacity. Section III describes the mathematical method. Results will be reported elsewhere by Christian, Stoeckly, and Schlueter.

II PHYSICAL FORMULATION

A. DIFFERENTIAL EQUATIONS

We denote mass density by ρ, fluid velocity by $\vec{v}$, specific internal energy (erg/gm) of the fluid by I, fluid pressure by P, temperature by T, the local acceleration due to gravity by $\vec{g} = -g\hat{e}_z$, and radiative energy flux density integrated over all frequencies by $\vec{F}_{rad}$ (erg/cm^2-sec). The conditions for mass balance, momentum balance, and energy balance of a volume element of fluid are

$$\frac{\partial \rho}{\partial t} = -\nabla\cdot(\rho\vec{v}), \tag{1}$$

$$\frac{\partial}{\partial t}(\rho\vec{v}) = -\nabla\cdot(\rho\vec{v}\vec{v}) - \nabla P + \rho\vec{g}, \tag{2}$$

$$\frac{\partial}{\partial t}(\rho I) = -\nabla\cdot(\rho I\vec{v}) - P\nabla\cdot\vec{v} - \nabla\cdot\vec{F}_{rad} - \rho D_{rad}, \tag{3}$$

where D_{rad} is the loss rate of thermal radiation per unit mass, which is discussed later in this subsection. Radiation pressure and radiant energy density are neglected.

Radiation Diffusion

During early time in many low-altitude fireballs, most of the radiant energy transfer is by photons whose mean free paths are much smaller than the fireball radius. The fractional temperature change over a few mean free paths is small for all frequencies that are significant at the given temperature. In such a region, the specific intensity is close to that for thermal equilibrium at that temperature, and we can treat the deviation from the equilibrium value

as a small quantity (approximation of local thermodynamic equilibrium (LTE), or radiation diffusion). This small quantity, which characterizes both the departure from a Planck spectral distribution and the departure from isotropy, is characterized by the radiative energy flux density.

The frequency spectrum of the radiative flux is, in LTE, a known function of the temperature and absorption coefficient of the fluid,

$$\vec{F}_\nu d\nu = -\frac{4\pi}{3}\frac{1}{(\kappa' + \kappa_s)\rho}\frac{\partial B_\nu}{\partial T}\nabla T\, d\nu,$$

where $\kappa'(\rho,T,\nu)$ is the mass absorption coefficient at frequency ν, corrected for stimulated emission, κ_s is the mass scattering coefficient, and $B_\nu(\nu,T)$ is the Planck function; the flux is greater at frequencies at which it experiences less absorption. One therefore needs only the integrated flux density, and the integration over frequency is done in the definition of the Rosseland mean opacity, $\kappa_R(\rho,T)$ (which, like κ', is in cm^2/gm). In this, the photon mean free path, $1/(\kappa' + \kappa_s)\rho$, is averaged over frequency with the weighting function $\partial B_\nu/\partial T$, which emphasizes high photon energies around $h\nu \approx 4kT$. The integrated radiative flux density is then

$$\vec{F}_{rad} = -\frac{16\sigma T^3}{3\kappa_R\rho}\nabla T, \tag{4}$$

where σ is the Stefan-Boltzmann constant. Since we use ρ and I as primary thermodynamic variables, we write this as

$$\vec{F}_{rad} = -K(\rho,T)\left[\left(\frac{\partial T}{\partial I}\right)_\rho \nabla I + \left(\frac{\partial T}{\partial \rho}\right)_I \nabla\rho\right], \tag{5}$$

where

$$K(\rho,T) \equiv 16\sigma T^3/3\kappa_R(\rho,T)\rho \tag{6}$$

is the radiative flux density per unit temperature gradient.

The cooler part of the burst region is far from LTE. Using the diffusion approximation in this region is inaccurate and can cause difficulties in obtaining a numerical solution. Therefore, we have diminished the LTE term of Eq. (3), $-\nabla\cdot\vec{F}_{rad}$, by using an artificially high Rosseland mean opacity for temperatures $kT \lesssim 0.7$ ev.

Radiation Loss From the Fireball

It is important to account in some way, however, for the radiant energy that leaves the heated region. We have allowed for such non-LTE radiative energy transfer by adding to Eq. (3) a radiative loss term, $-\rho D_{rad}$, which is explained in this subsection. This radiative loss term transfers radiant energy from a volume element to infinity (outside the heated region), whereas the LTE term transfers radiant energy only between adjacent volume elements.

The spontaneous emission per unit mass per unit time per unit solid angle emitted in frequency interval $d\nu$ from an element of fluid is

$$j_\nu d\nu = \kappa' B_\nu d\nu,$$

where again $\kappa'(\rho,T,\nu)$ is the mass absorption coefficient corrected for stimulated emission, and $B_\nu(\nu,T)$ is the Planck function. To escape completely from the fireball, the emission traveling in direction $\hat{u}$ traverses a path $L(\hat{u})$ from the radiating element to outside the fireball (see Fig. 1); the fraction that survives this traversal is $\exp[-\tau_\nu(\hat{u})]$, where

$$\tau_\nu(\hat{u}) \equiv \int_{L(\hat{u})} \kappa'(\rho,T,\nu)\,\rho\,d\ell$$

is the optical depth for frequency ν along the path $L(\hat{u})$.

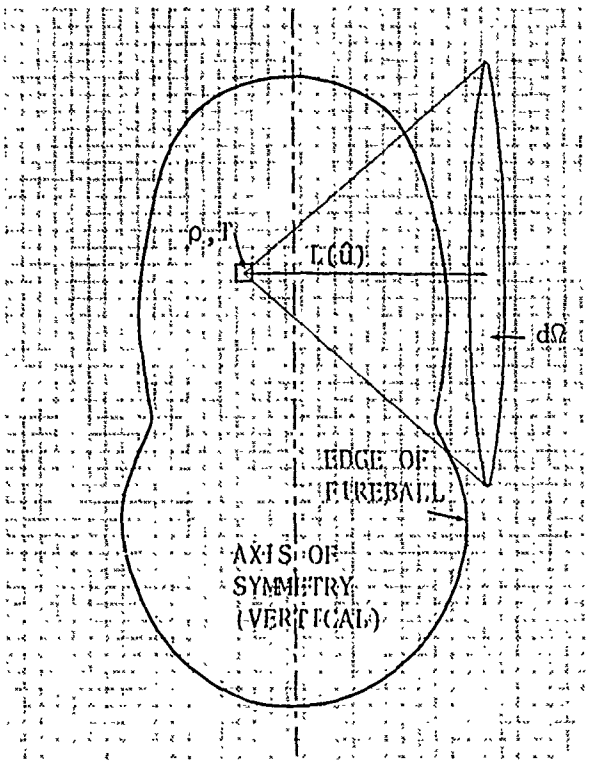

Figure 1. Axial cross section of interacting fireballs, showing geometry used to calculate radiation loss. The power emitted by a fluid element into solid angle $d\Omega$ about a direction $\hat{u}$ is assumed to travel along the path $L(\hat{u})$. Before escaping from the composite fireball, this power is attenuated by a factor $\exp[-\tau(\hat{u})]$. (The dotted squares are the cells used in a representative two-burst problem. The composite fireball shape results from independent bursts at different times and places.)

Stimulated emission is included here by combining it with the spontaneous emission that caused it; it is correctly included in the fraction $\exp[-\tau_\nu(\hat{u})]$ by the correction for stimulated emission in κ' in the above equation.

We consider the frequency interval $0 < h\nu < 4.13$ ev because it includes most of the radiation escaping from a low-altitude fireball; this interval includes the infrared, visible, and near ultraviolet (wavelengths > 3000 Å) and is referred to here as "thermal." In

integrating over frequency, it is convenient to use the Planck (or "emission") mean opacity for this frequency range, defined by

$$\kappa_{p4}(\rho,T) \equiv \int_0^{4.13\ ev} \kappa'(\rho,T,\nu)\ B_\nu(\nu,T)\ d\nu \Big/ \int_0^{4.13\ ev} B_\nu(\nu,T)\ d\nu. \tag{7}$$

The spontaneous thermal emission per unit mass per unit time per unit solid angle emitted by a fluid element is therefore

$$j_4(\rho,T) = \int_0^{4.13\ ev} \kappa'(\rho,T,\nu)\ B_\nu(\nu,T)\ d\nu,$$

$$= \kappa_{p4}(\rho,T)\ f_4(T)\ \sigma T^4/\pi, \tag{8}$$

where the integral of the Planck function over this frequency range is written as $f_4(T)\ \sigma T^4/\pi$. The function $f_4(T)$ is taken from Allen's table (Ref. 2). To find how much of this thermal emission escapes from the fireball, we make the approximation that

$$\int_0^{4.13\ ev} j_\nu \exp[-\tau_\nu(\hat{u})]\ d\nu \approx j_4 \exp[-\tau(\hat{u})],$$

where

$$\tau(\hat{u}) \equiv \int_{L(\hat{u})} \kappa_{p4}(\rho,T)\,\rho\ d\ell \tag{9}$$

is the (Planck) mean optical depth for this frequency range along the path $L(\hat{u})$. This approximation of using a single attenuation factor over the whole frequency range becomes less serious as the fireball grows optically thin.

Integrating over all directions then gives the loss rate per unit mass of thermal radiation (erg/gm/sec) from a fluid element,

$$D_{rad} = j_4 \int_{4\pi} \exp[-\tau(\hat{u})]\, d\Omega, \qquad (10)$$

where $d\Omega$ denotes an element of solid angle about the fluid element. The factor j_4 is outside the integral because spontaneous emission is isotropic.

Eqs. (5), (8), (9), and (10) replace $\vec{F}_{rad}$ and D_{rad} in Eq. (3). Then, for problems having symmetry about the vertical axis, the system of Eqs. (1) to (3) consists of four component integro-differential equations for the variables ρ, I, v_r, and v_z.

B. EQUATIONS OF STATE AND OPACITY

To complete the problem, we must specify algebraic or tabular relations for these properties of air of sea-level composition: fluid pressure $P(\rho,I)$, temperature $T(\rho,I)$, Rosseland mean opacity $\kappa_R(\rho,T)$, and Planck mean opacity for the frequency range $0 < h\nu < 4.13$ ev, $\kappa_{P4}(\rho,T)$.

Equations of state for air are needed to determine fluid pressure $P(\rho,I)$ and temperature $T(\rho,I)$ in terms of density ρ and specific internal energy I. Our equation of state, written by D. Sappenfield, uses data from Hilsenrath and others (Refs. 3 and 4) for $1500° \leq T \leq 5\times10^6$ °K ($0.13 \leq kT \leq 430$ev), data from Gilmore (Ref. 5) for $T = 1000$ °K, and relations for an ideal diatomic gas with no vibrational excitation for $T \leq 500$ °K. The zero of internal energy refers to gaseous N_2 and O_2 at $T = 0°K$.

Data tables are used to do two-dimensional linear interpolation with log ρ, ℓn I, ℓn T, and P/ρI as variables. To save computation, we use this routine to make larger data tables (10 densities by 75 internal energies) in which we do two-dimensional linear interpolation with ρ, I, T, and P/ρI as variables. From this interpolation we also get the derivatives like $(\partial T/\partial I)_\rho$ for Eq. (5); these are piecewise constant. Figs. 2 and 3 present the two equation of state relations in a more conventional form, showing I and P/ρI as functions of temperature for several densities.

The Rosseland mean opacity of air is calculated from an analytic relation of Brode (Ref. 6); this is plotted in Fig. 4. The maxima near $kT \approx 6$ ev occur because, for $kT < 2$ ev, few photons have enough energy to ionize air, while for $kT > 10$ ev, ionization has greatly reduced the number of bound electrons. Figure 5 shows the corresponding photon mean free path, $\lambda_R(\rho,T) = 1/\kappa_R(\rho,T)\rho$. Brode's relation gives an artificially high opacity at low temperatures ($kT \lesssim 0.7$ ev) for the reason mentioned on page 7. Computing time for this formula was reduced by 60% by recoding.

The Planck mean opacity of air, averaged over the photon energy range $0 < h\nu < 4.13$ ev, is taken from Sowle and others (Ref. 7, pg. 10) in the form of tables of $\kappa_{P4}(\rho,T)$. Again, Fig. 6 shows this opacity, and Fig. 7 shows the corresponding mean free path, $\lambda_{P4}(\rho,T) = 1/\kappa_{P4}(\rho,T)\rho$. This opacity, like the Rosseland opacity above, includes the correction for stimulated emission. As before, these data tables are expanded by two-dimensional linear interpolation with $\ell n\ \rho$, ℓn T, and $\ell n\ \kappa_{P4}$ as variables; this larger table is used to do two-dimensional linear interpolation with ρ, T, and κ_{P4} as variables.

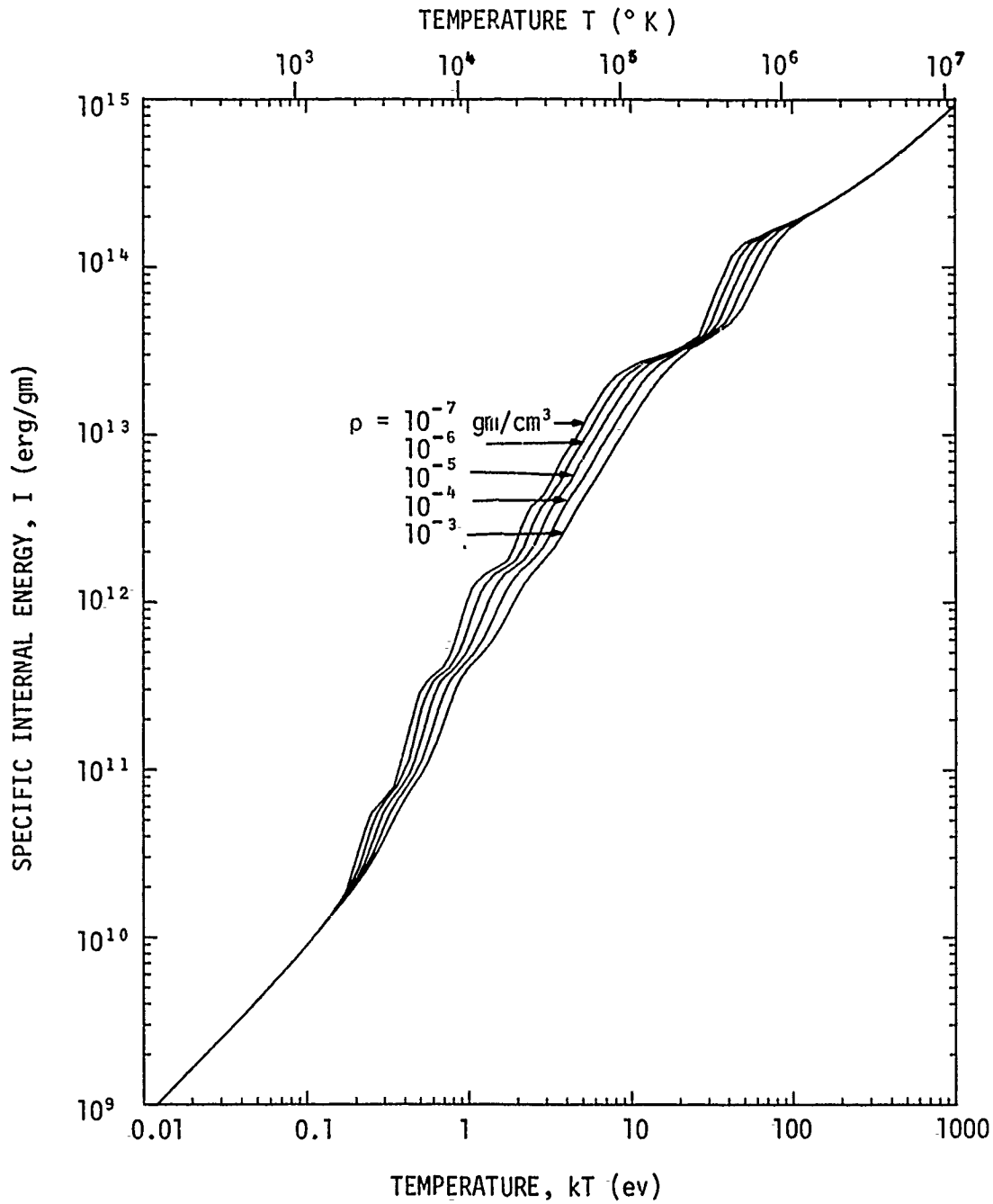

Figure 2. Specific internal energy of air in thermal equilibrium as a function of temperature for various densities.

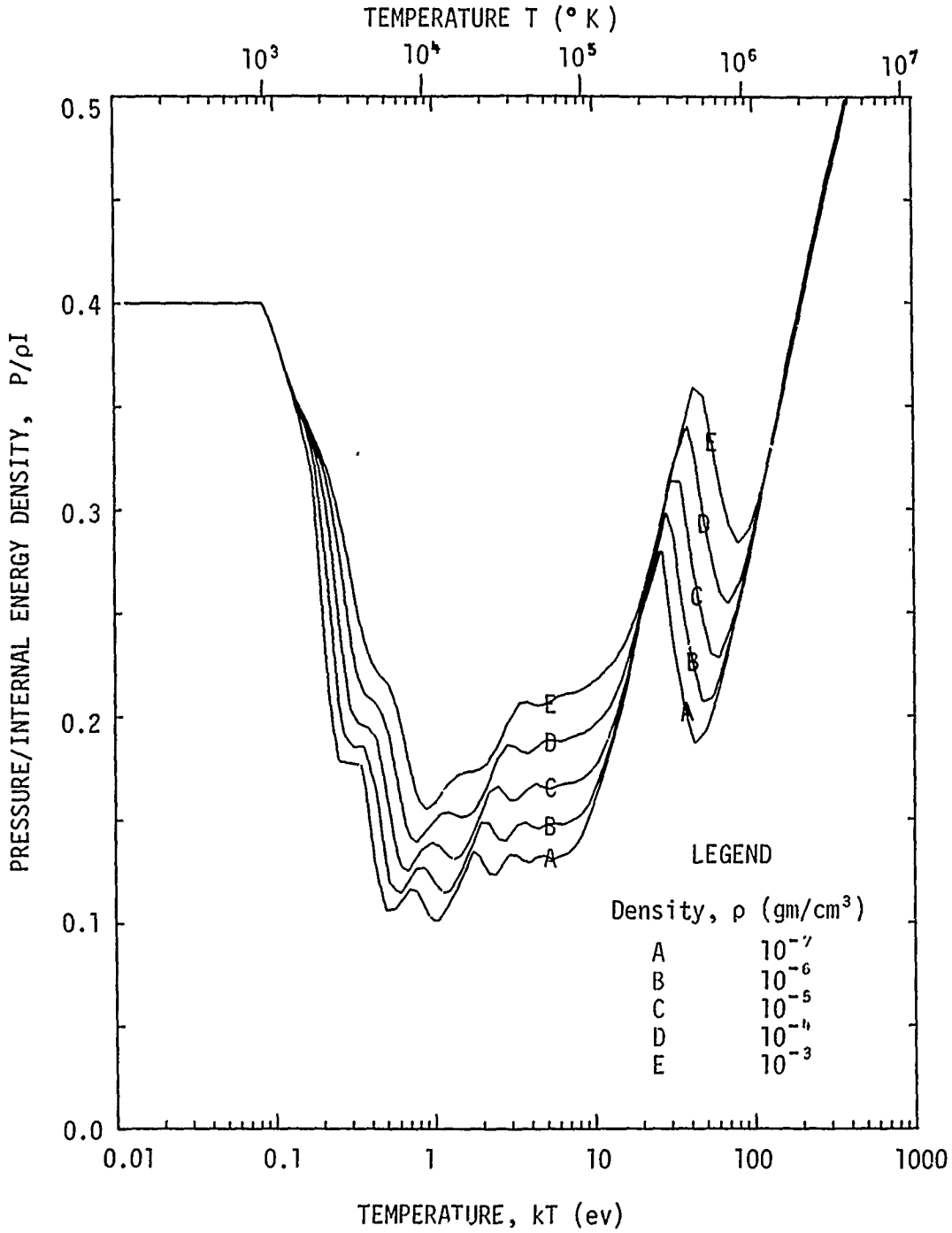

Figure 3. Dimensionless pressure of air in thermal equilibrium as a function of temperature for various densities.

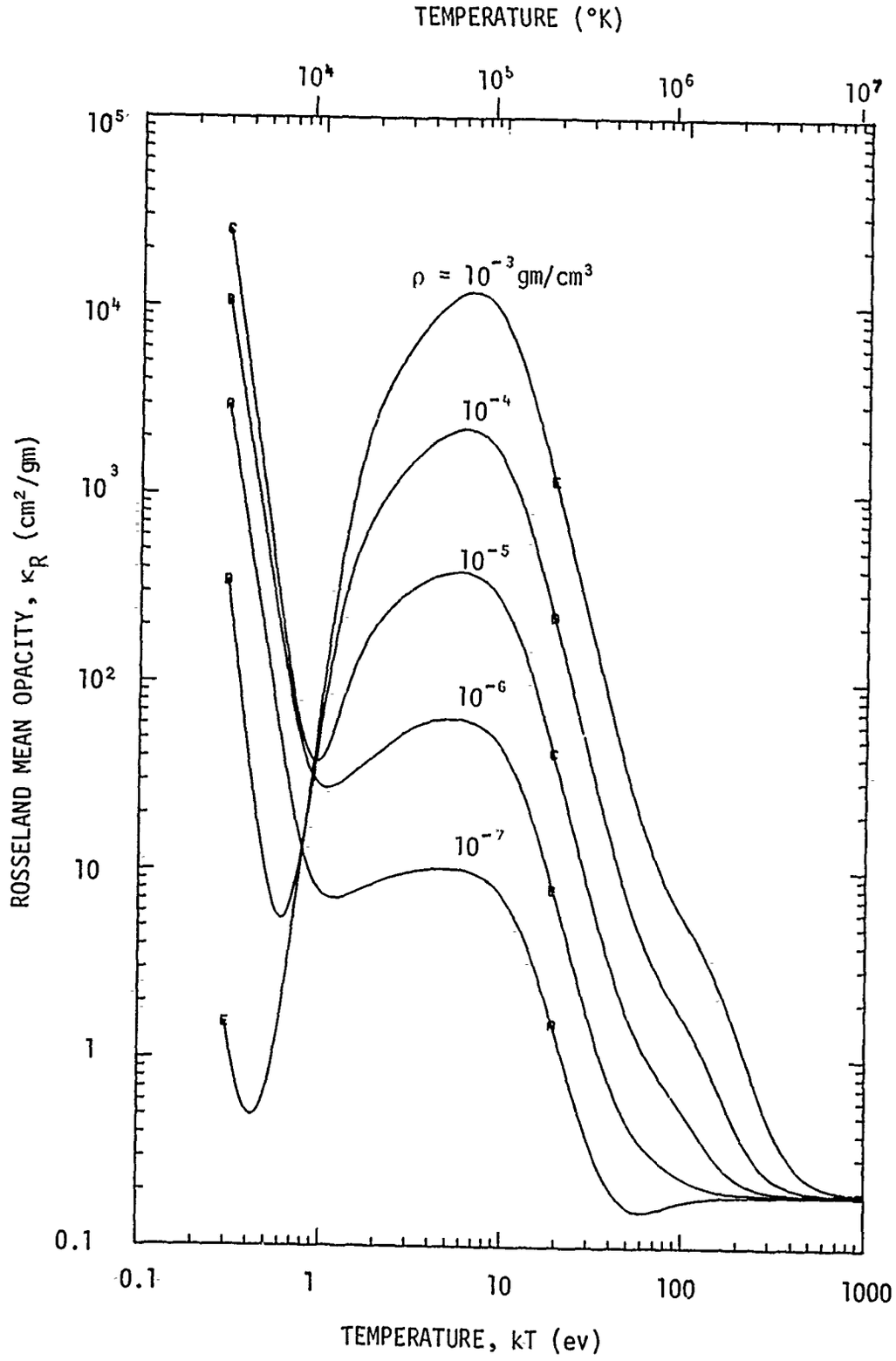

Figure 4. Rosseland mean opacity of air as a function of temperature for various densities. The high opacity before the first minimum (at kT ≈ 0.4 to 1 ev) is artificial (see pg. 7).

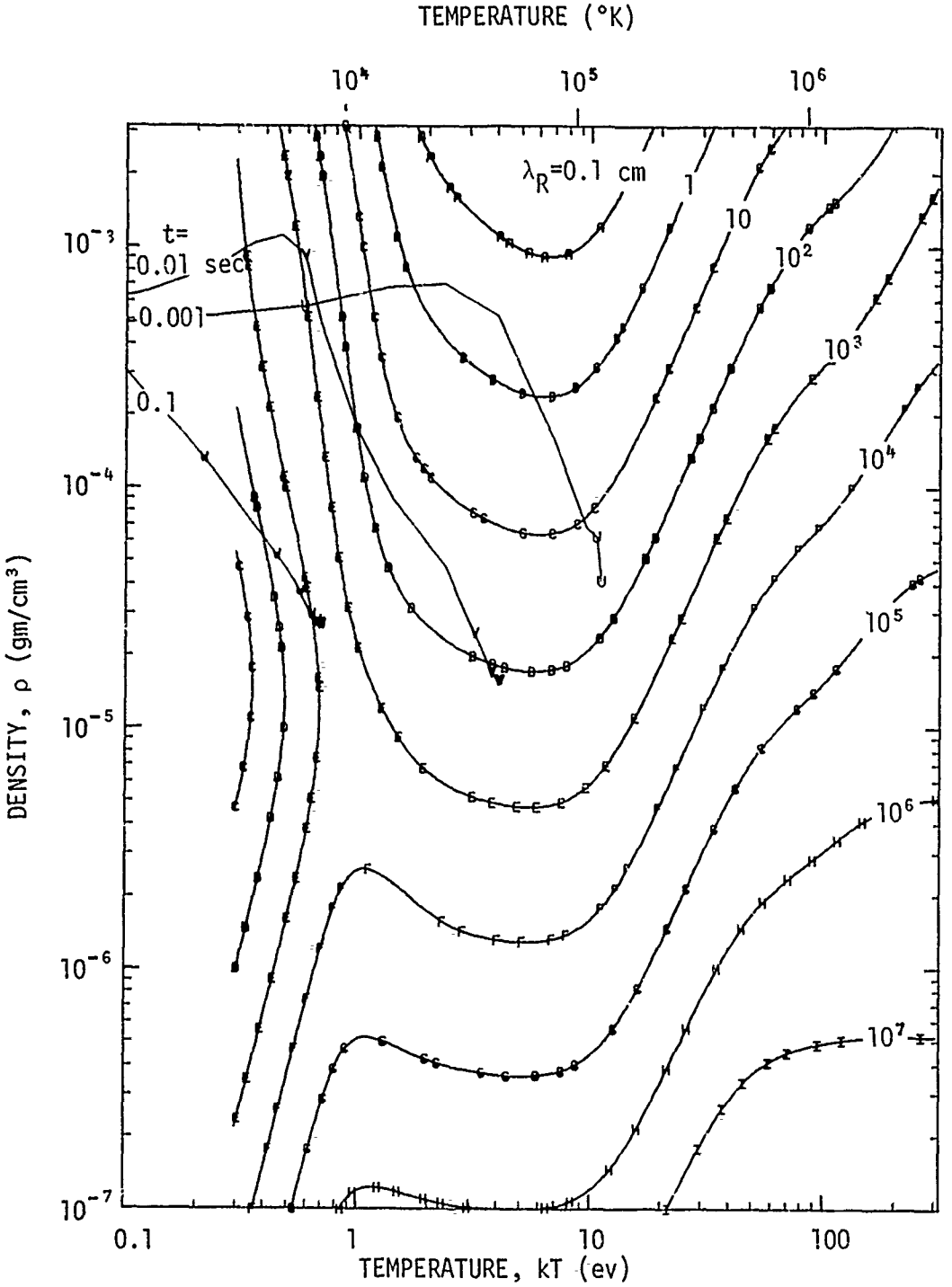

Figure 5. Contour plot in the density-temperature plane of the mean free path of photons in air (based on the Rosseland mean opacity). This plot shows the data of Fig. 4 in the form $\lambda_R(\rho,T) = 1/\kappa_R(\rho,T)\rho$. For comparison we show a burst of 5 kt energy at altitude 9.1 km; the line curves show conditions at three times after this burst.

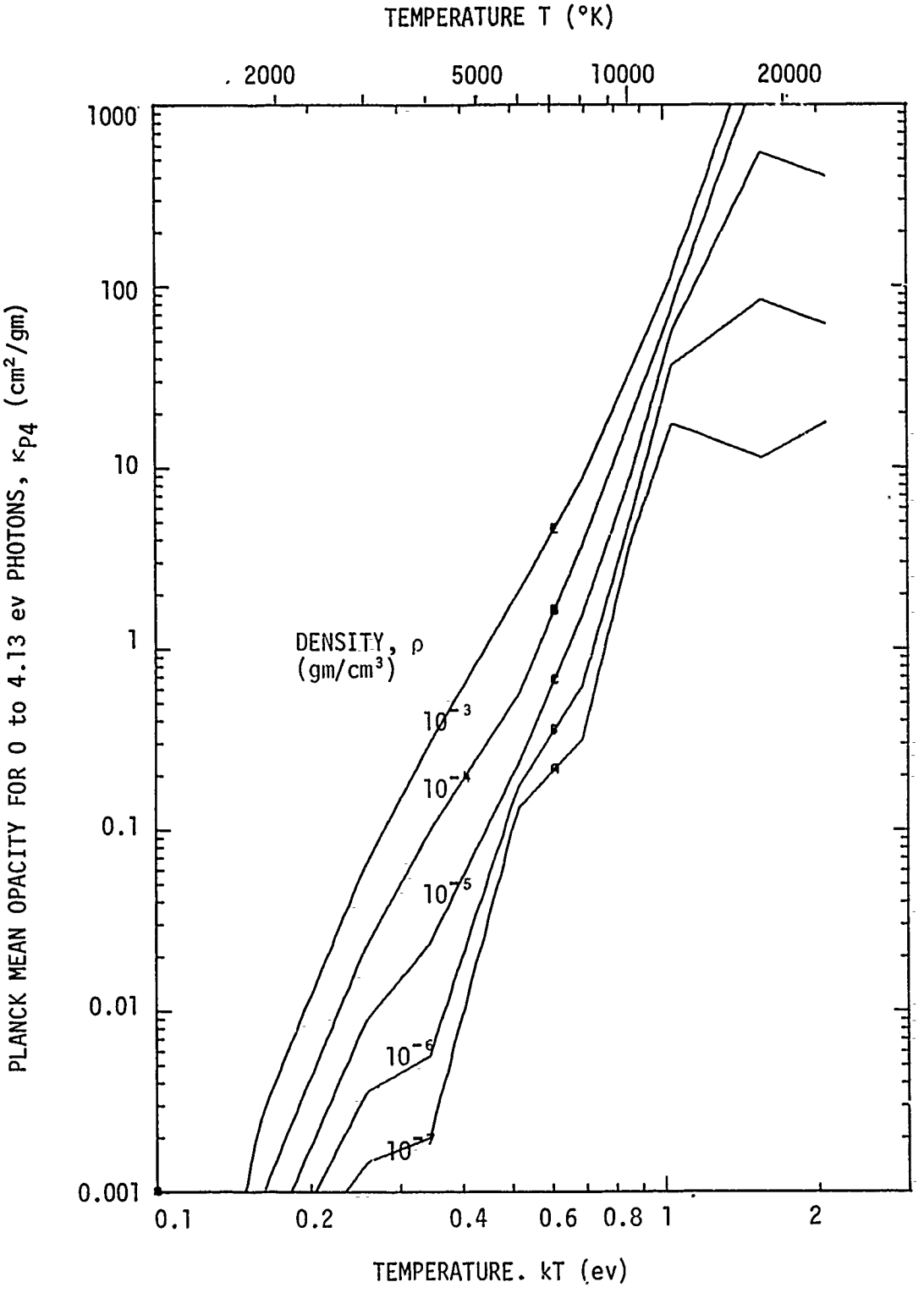

Figure 6. Planck mean opacity of air as a function of temperature for various densities. The opacity is averaged over the photon energy range $0<h\nu<4.13$ ev (wavelengths > 3000Å).

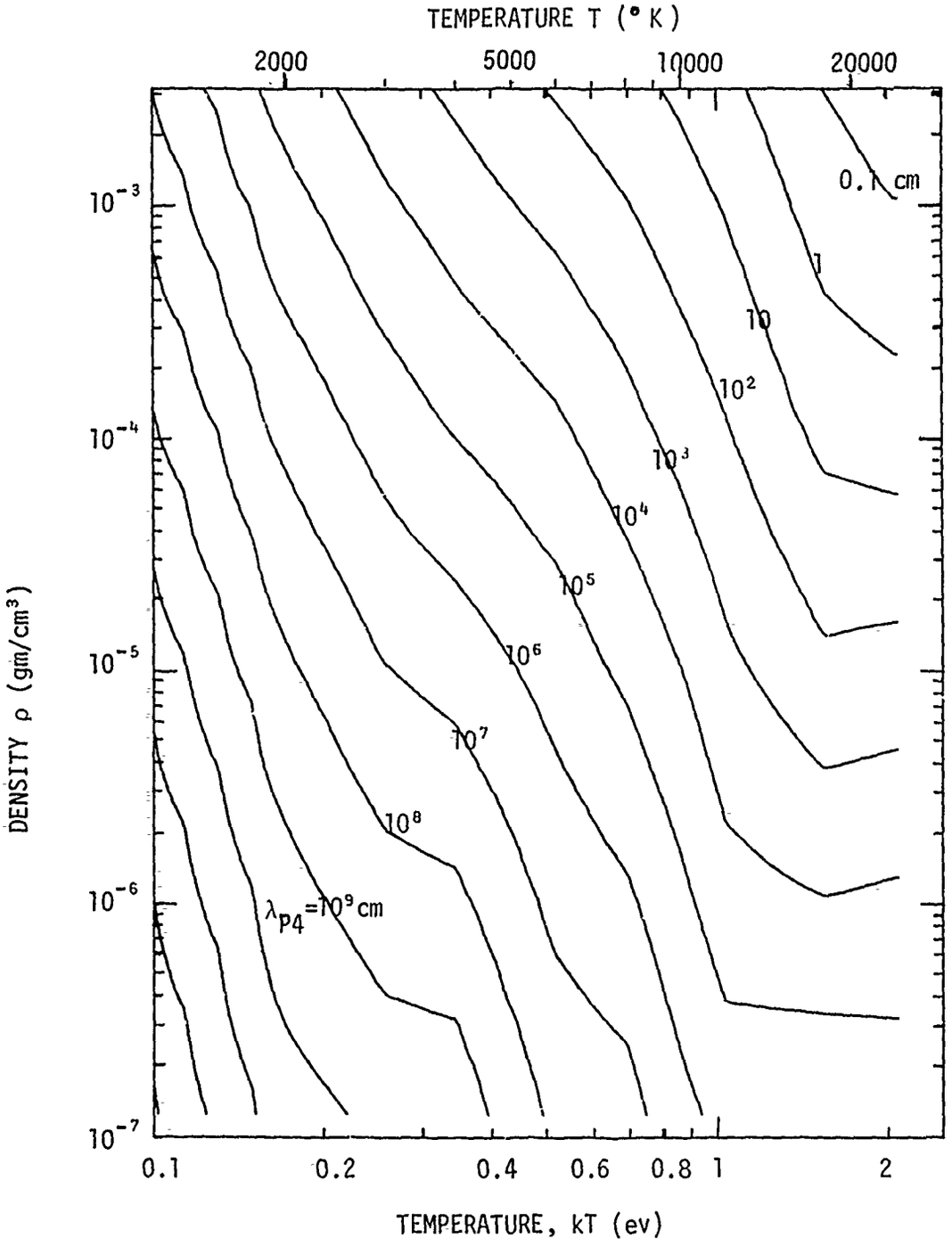

Figure 7. Contour plot in the density-temperature plane of the mean free path of photons in air (based on the Planck mean opacity for photon energy range 0 to 4.13 ev). This plot shows the data of Figure 6 in the form $\lambda_{P4}(\rho,T) = 1/\kappa_{P4}(\rho,T)\rho$.

C. INITIAL AND BOUNDARY CONDITIONS

Undisturbed Atmosphere

At low altitudes, the dependence of mass density $\rho(z)$ on altitude z is from the 1962 U.S. Standard Atmosphere (Ref. 8). The pressure just above the top of the grid is also taken from this source, and pressures $P(z)$ at lower altitudes are obtained by integrating the hydrostatic equilibrium equation. The acceleration due to gravity is $g(z) = g_0 R_0^2/(R_0 + z)^2$, where $g_0 = 980.665$ cm/sec^2 and $R_0 = 6.37817 \times 10^8$ cm. The specific internal energy is then $I(z) = P(z)/0.4\ \rho(z)$. The curvature of the earth is neglected.

Deposition of Initial X-rays

The initial X-rays are characterized by an energy spectrum $J(\varepsilon)$, defined so that the X-ray energy in the photon energy interval $d\varepsilon$ is $J(\varepsilon)\, d\varepsilon$. We usually use a Planck spectrum characterized by some temperature T_x and total energy E_x,

$$J(\varepsilon)\, d\varepsilon = \frac{C\, \varepsilon^3\, d\varepsilon}{\exp\,(\varepsilon/kT_x) - 1} \quad \text{for } \varepsilon > 0.013 \text{ kev}, \tag{11}$$

where the constant C normalizes the total X-ray energy:

$$\int_{0.013\ \text{kev}}^{\infty} J(\varepsilon)\, d\varepsilon = E_x. \tag{12}$$

The X-rays, assumed to come from a point source, could be further characterized by an angular distribution, which we currently take to be isotropic.

We consider energy loss of these X-rays only by photon absorption; Compton scattering is ignored. The problem is to calculate the change of specific internal energy ΔI of air caused by deposition of X-ray energy along rays from the burst point on which the density is given. Our deposition routine, written by D. Glenn, uses the method of Sappenfield and Tierney (Ref. 7, pp. 3 to 8); the part relevant at low altitude is described below.

For air that is not fully ionized, our corrected mass absorption coefficient is

$$\kappa'(\varepsilon) = \begin{cases} k_1/\varepsilon^3 & \text{for } \varepsilon > 0.4 \text{ kev}, \\ k_2/\varepsilon^{2.15} & \text{for } 0.013 < \varepsilon < 0.4 \text{ kev}, \end{cases} \tag{13}$$

where $k_1 = 3620$ cm^2-kev^3/gm and $k_2 = 369$ cm^2-kev$^{2.15}$/gm; Fig. 8 shows this absorption coefficient. The first part of this relation is based on data of McMaster (Ref. 9); the second part is close to data for molecular oxygen in the DNA Reaction Rate Handbook (Ref. 10). This rough absorption coefficient includes no dependence on the density of the air and none (except as in the next paragraph) on its temperature.

For air that is fully ionized by X-rays, we assume that the resulting photoelectrons thermalize in a time shorter than that (a few microseconds) during which the initial X-rays are emitted by the debris. That is, the photoelectrons resulting from the earliest X-rays from the debris quickly undergo collisions that free other electrons and spread the energy, returning the air toward thermal equilibrium. When all electrons in a region have been so freed and so no further (net) X-ray absorption can occur, the specific internal energy of the air there has reached an upper limit. This limit is the internal energy at which air close to thermal equilibrium is nearly fully ionized, or about $I^* = 3 \times 10^{14}$ erg/gm. We use this limit in determining an

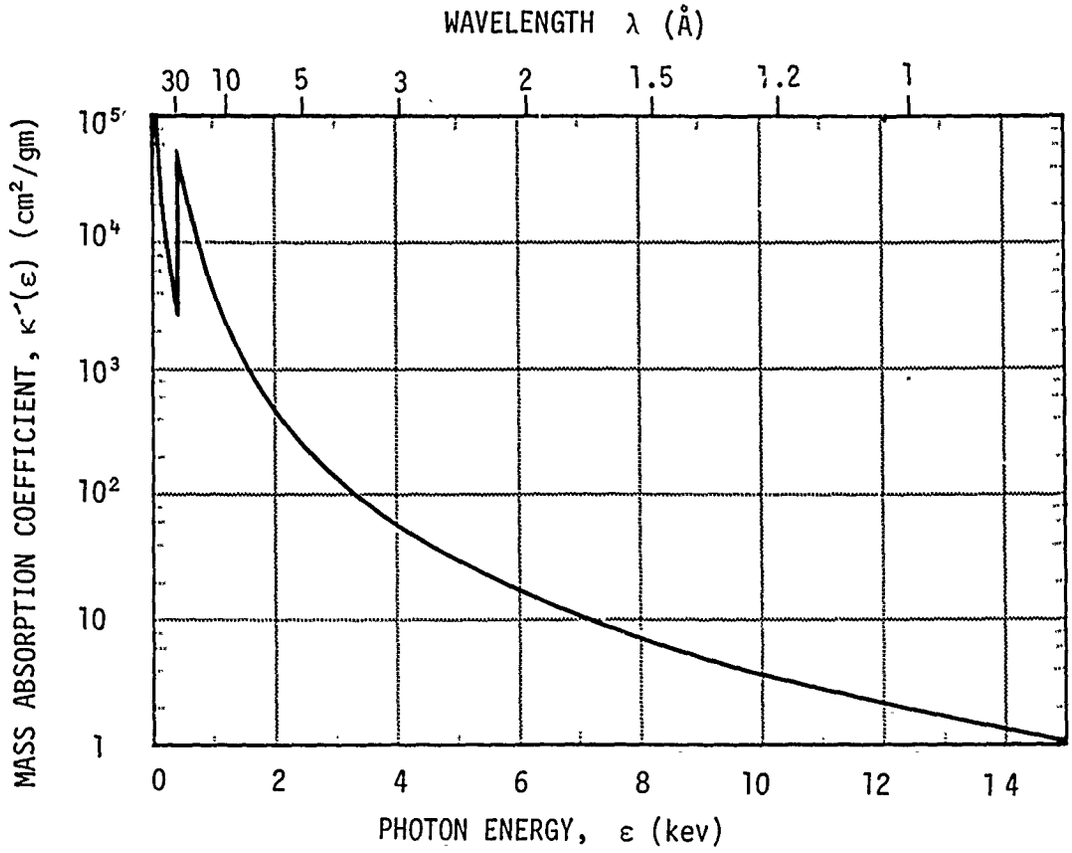

Figure 8. Mass absorption coefficient of incompletely ionized air vs. photon energy. The absorption edge is at the energy of the K absorption edge of nitrogen.

effective mass absorption coefficient for air that becomes fully ionized:

$$\kappa^*(\varepsilon) = \begin{cases} k^*/\varepsilon^3 & \text{for } \varepsilon > 0.4 \text{ kev}, \\ 0 & \text{for } \varepsilon < 0.4 \text{ kev}, \end{cases} \tag{14}$$

where k^* is a constant ($k^* \leq k_1$) to be determined by the condition that the specific internal energy not exceed I^* (k^* and R^* will be determined together through iteration with Eqs. 18 and 15). For simplicity we assume that photons of energy less than 0.4 kev are not absorbed in the fully ionized region; these photons carry only a small part of the energy from most sources of interest.

We determine first the size of the region in which air becomes fully ionized. For simplicity we assume that this region is a sphere; that the density in it is a constant, the current burst-point air density ρ_0; and that the specific internal energy in it initially is negligible compared to I^*. The radius R^* of this region is determined by balancing the energy absorbed in this sphere with its net energy intake:

$$I^* \rho_0 \frac{4}{3} \pi R^{*3} = \int_{0.4\ \text{kev}}^{\infty} J(\varepsilon) \left[1 - \exp\left(- \kappa^*(\varepsilon)\ \rho_0\ R^*\right)\right] d\varepsilon. \qquad (15)$$

By assumption (Eq. 14), photon energies below 0.4 kev do not contribute.

Outside the fully ionized region, we calculate the X-ray energy deposition in spherical coordinates (r, θ) centered at the burst point and later transform the results to the desired grid. The angle θ is measured from the vertical. In this region the unabsorbed X-ray energy in energy interval $d\varepsilon$ that crosses unit area at a distance r is

$$F_\varepsilon(r,\theta,\varepsilon)\, d\varepsilon = \frac{J(\varepsilon)\, d\varepsilon}{4\pi r^2} \exp\left[- \kappa^*(\varepsilon)\ \rho_0\ R^* - \kappa'(\varepsilon) \int_{R^*}^{r} \rho(r',\theta)\, dr'\right] \qquad (16)$$

$$\text{for } r \geq R^*,$$

where $\rho(r, \theta)$ is the current mass density, which may have been altered by a previous burst. The energy per unit mass deposited at position (r, θ) is then

$$\Delta I\ (r,\ \theta) = \begin{cases} I^* & \text{for } r < R^*, \\ \displaystyle\int_{0.013\ \text{kev}}^{\infty} \kappa'(\varepsilon)\ F_\varepsilon(r,\ \theta,\ \varepsilon)\, d\varepsilon & \text{for } r > R^*. \end{cases} \qquad (17)$$

Continuity of $\Delta I(r, \theta)$ at the boundary requires that

$$I^* \approx \int_{0.4\ \text{kev}}^{\infty} \kappa'(\varepsilon)\ F_\varepsilon(R^*, \theta, \varepsilon)\ d\varepsilon; \qquad (18)$$

the contribution to this integral from energies below 0.4 kev is ignored for simplicity. We determine k^* and R^* simultaneously from conditions (18) and (15) by iteration; after that the deposition of X-ray energy by Eq. (17) is straightforward.

Our deposition outside the fully ionized region uses 25 angular zones ($\Delta\theta = 7°.5$) and 50 nonuniform radial zones. The transformation back to the original grid uses two-dimensional linear interpolation with r, θ, and $\log\ \Delta I(r,\theta)$ as variables. The integral $\int_{R^*}^{r} \rho(r',\theta)dr$ is evaluated by the trapezoidal rule.

Initial Debris Energy

The debris is characterized by its mass M_d (if this is important) and its initial kinetic energy K_d. Large velocity gradients near the burst point cause difficulties in our numerical method, however, so we elect to convert this kinetic energy immediately to internal energy. This procedure seems acceptable because the results show an appropriate partition of the total energy in the problem between kinetic and internal by 2 or 3 msec after the burst. The debris mass (if any) and internal energy are initially deposited uniformly through a sphere of radius R_0, which we choose; typically R_0 is a few times the initial cell size.

Boundary Conditions

As long as the outer boundary is well outside the fireball, radiation diffusion is unimportant there. We have made the simple approximation, which has been satisfactory, that radiation diffusion causes no heating or cooling of the fluid at the outer boundary, $\nabla \cdot \vec{F}_{rad} = 0$. The general regridding capability enables this outer boundary (in the shape of a cylinder, or sphere) to be moved to keep it well outside the fireball(s).

The hydrodynamic part of the boundary conditions must allow shocks to pass through the outer boundary smoothly, without creating artificial reflected waves at the boundary. At this boundary we assume (1) that there is no inflow of mass, and (2) that the time rate of change of the amplitude of certain incoming waves is zero (see Ref. 1, Appendix C). We allow shocks to pass through the boundary when they become moderate to weak, and these conditions seem to give satisfactory results.

III MATHEMATICAL TECHNIQUE

A. DIFFERENCE EQUATIONS

For problems having symmetry about the vertical axis, the system of equations (1) to (3) consists of four component integro-differential equations for the variables ρ, I, v_r, and v_z. Each is first order in time and space, except that radiation diffusion makes Eq. (3) second order in the spatial variables. The MICE code solves this system by a modified Lax-Wendroff method; the method uses the technique of time-step splitting and is modified to be implicit. Our treatment of radiation involves further time-step splitting (see Eqs. 19) and is also implicit (except for the radiation loss term, which involves integrals).

The difference equations are written in two-dimensional cylindrical coordinates (r,z). A (nonuniform) grid of J_r by J_z spatial cells is specified, with boundaries $r_{k-1/2}$($k=1,\ldots,J_r+1$) and $z_{\ell-1/2}$($\ell=1,\ldots,J_z+1$). The coordinates of the cell centers are denoted by r_k ($k=1,\ldots,J_r$) and z_ℓ ($\ell=1,\ldots,J_z$).[1] The choice of cell boundaries is arbitrary (Sec. III-C gives our criteria); however, if adjacent cells differ in width by more than 10 or 20 percent for a time long enough for their contents to interact, the results are degraded. The code is limited to $J_z \leq 98$ cells vertically (which give a maximum of about 5000 cells). For the case plotted in Fig. 5 and for those mentioned in Sec. IV, the cell size in the fireball(s) ranges from 3 × 3 meter at burst time to 20 × 20 mete. (at most) after a few hundredths of a second.

---

[1] We wish to make $r_1 = 0$, so we treat the axis cells specially, defining $r_{1/2} = 0$.

The dependent variables are advanced in time by application of four difference operators, R_r, R_z, L_r, and L_z, that are one-dimensional (that is, each operator involves differences in only one direction, specified by its subscript). These operators are applied sequentially instead of simultaneously (time-step splitting). In describing this, we denote dependent variables such as $\rho(r_k, z_\ell, t^n)$ by $\rho^n_{k,\ell}$ etc., and consider the collection of dependent variables at all grid points at time t^n to be a vector, having $4\,J_r J_z$ components:

$$\underline{U}^n \equiv (\rho^n_{k,\ell},\ I^n_{k,\ell},\ (v_r)^n_{k,\ell},\ (v_z)^n_{k,\ell},\quad k=1,\ldots,J_r;\ \ell=1,\ldots,J_z).$$

We define three successive sets of intermediate variables, each resulting from the application of one more matrix difference operator:

$$\begin{aligned}
\underline{U}^{n,r} &\equiv \underline{U}^n + R_r(\underline{U}^n, \underline{U}^{n,r}),\\
\underline{U}^{n,rz} &\equiv \underline{U}^{n,r} + R_z(\underline{U}^{n,r}, \underline{U}^{n,rz}),\\
\underline{U}^{n,rz\rho} &\equiv \underline{U}^{n,rz} + L_r(\underline{U}^{n,rz}, \underline{U}^{n,rz\rho}).
\end{aligned} \tag{19}$$

Finally the last operator yields the time-advanced variables:

$$\underline{U}^{n+1} \equiv \underline{U}^{n,rz\rho} + L_z(\underline{U}^{n,rz\rho}, \underline{U}^{n+1}).$$

Without the latter of the two operands in parentheses, each such equation would represent a collection of $4J_rJ_z$ explicit equations; with it, each equation is implicit and represents a system of $4J_rJ_z$ simultaneous algebraic equations for that same number of variables.

Basically, changes in the variables due to hydrodynamic terms on the right sides of Eqs. (1) to (3) are accomplished by the L_r and L_z operators, and changes due to the radiation terms of Eq. (3) are

accomplished by R_r and R_z. L_r and L_z are the "L_r phase 2" and "L_z phase 2" operators of Fajen (Ref. 1, pp. 18-23); his "L phase 1" operators are unnecessary in the absence of a magnetic field. The R_r and R_z operators affect only the $I_{j,k}$ and not densities or velocities (because radiation terms appear only in the energy equation, (3)). Thus, the R_r difference operator consists of linear difference equations, one for each cell (k,ℓ), that relate $I^{n,r}_{k-1,\ell}$, $I^{n,r}_{k,\ell}$, and $I^{n,r}_{k+1,\ell}$ with known quantities.

The R_r and R_z operators are defined together (in Eqs. 20 and 21), using the following abbreviated notation. The coordinate x can be either r or z, and we retain only the subscript denoting the x coordinate. For example, I^n_j and $I^{n,x}_j$ denote $I^n_{j,\ell}$ and $I^{n,r}_{j,\ell}$ if $x = 4$; if $x = z$ they denote $I^{n,r}_{k,j}$ and $I^{n,rz}_{k,j}$ (the second superscript is abbreviated in this case). The cell widths and the distances between cell centers are denoted by $\Delta x_j \equiv x_{j+1/2} - x_{j-1/2}$ and $\Delta x_{j+1/2} \equiv x_{j+1} - x_j$, respectively, and d_{j+1} is a space interpolation coefficient, $d_{j+1} \equiv (x_{j+1/2} - x_j)/(x_{j+1} - x_j)$. The index m used in representing divergences is 1 for the r direction and 0 for the z-direction.[2] The specific heat capacity is denoted by $c_v \equiv (\partial I/\partial T)_\rho$, and functions of thermodynamic variables are abbreviated as $T^n_j = T(I^n_j, \rho^n_j)$, $K^n_j = K(\rho^n_j, T^n_j)$, etc. A time interpolation coefficient θ allows the R operators to be explicit ($\theta=0$) or implicit ($0<\theta\leq 1$); we use $\theta=1$. (We tried $\theta=0$ but had difficulties.)

In representing the radiative flux density, note that in Eq. (5) the second term in the brackets is generally small compared to the first because $T(I,\rho)$ depends only weakly on ρ (see Fig. 2). We therefore treat $\partial\rho/\partial x$ less elaborately than $\partial I/\partial x$ here. The parallel component of the radiative flux density F_x at a cell boundary is represented as

---

[2] In spherical coordinates m - 2 for the r direction; in Cartesian coordinates m = 0 for all directions.

$$\left(F_x\right)_{j+1/2}^{n+1/2} \equiv -\left(\frac{K}{c_v}\right)_{j+1/2}^{n} \frac{\left[(1-\theta)\left(I_{j+1}^{n}-I_j^{n}\right) + \theta\left(I_{j+1}^{n,x}-I_j^{n,x}\right)\right]}{\Delta x_{j+1/2}}$$

$$-\left[K\left(\frac{\partial T}{\partial \rho}\right)_I\right]_{j+1/2}^{n} \frac{\left(\rho_{j+1}^{n}-\rho_j^{n}\right)}{\Delta x_{j+1/2}} \quad ,$$

and the coefficients composed of quantities at cell boundaries are evaluated by linear spatial interpolation,

$$\left(F_x\right)_{j+1/2}^{n+1/2} = -\frac{1}{\Delta x_{j+1/2}}\left(\frac{d_{j+1}\,K_{j+1}^{n}}{(c_v)_{j+1}^{n}} + \frac{\left(1-d_{j+1}\right)K_j^{n}}{(c_v)_j^{n}}\right)\left[(1-\theta)\left(I_{j+1}^{n}-I_j^{n}\right) + \theta\left(I_{j+1}^{n,x}-I_j^{n,x}\right)\right]$$

$$-\frac{1}{\Delta x_{j+1/2}}\left[d_{j+1}K_{j+1}^{n}\left(\frac{\partial T}{\partial \rho}\right)_{I,j+1}^{n} + \left(1-d_{j+1}\right)K_j^{n}\left(\frac{\partial T}{\partial \rho}\right)_{I,j}^{n}\right]\left(\rho_{j+1}^{n}-\rho_j^{n}\right)$$

$$\text{for } 1\tfrac{1}{2} \le j+\tfrac{1}{2} \le J_x-\tfrac{1}{2}\,. \qquad (20)$$

The radiation terms in the energy balance (Eq. 3) are complicated by the integral in D_{rad} (Eq.10). This is treated in the next subsection; the part of D_{rad} that is included in the R_x operator is denoted by $(D_x)_j^n$, given by Eq.(29). The effect of the radiation terms on the energy balance (Eq.3) is then represented by

$$\frac{I_j^{n,x}-I_j^{n}}{\Delta t^{n+1/2}} = -\frac{1}{\rho_j^{n}}\,\frac{\left[x_{j+1/2}^{m}\left(F_x\right)_{j+1/2}^{n+1/2} - x_{j-1/2}^{m}\left(F_x\right)_{j-1/2}^{n+1/2}\right]}{x_j^{m}\,\Delta x_j} - \left(D_x\right)_j^{n}$$

$$\text{for} \quad 2 \le j \le J_x-1, \qquad (21)$$

where $\Delta t^{n+1/2} = t^{n+1} - t^{n}$ is the time step.

Two boundary conditions complete the system of equations (21). At the outer boundary, well outside the fireball, radiation diffusion causes no heating or cooling of the fluid, $\nabla\cdot\vec{F}_{rad} = 0$. At the outside ($k=J_r$) and top ($\ell=J_z$) this condition is

$$\frac{I^{n,x}_{J_x} - I^{n}_{J_x}}{\Delta t^{n+1/2}} = - (D_x)^n_{J_x} . \tag{22}$$

The other condition, which applies at the bottom ($\ell=1$) and at the axis ($k=1$), includes the symmetry requirement at the axis:

$$\frac{I^{n,x}_1 - I^n_1}{\Delta t^{n+1/2}} = \begin{cases} - (D_x)^n_1 - \dfrac{1}{\rho^n_1} \dfrac{(m+1)}{(r_{3/2} - 0)} (F_x)^{n+1/2}_{3/2} & \text{if } x = r, \\ - (D_x)^n_1 & \text{if } x = z. \end{cases} \tag{23}$$

Equations (21) to (23), with the substitution (20), form a set of J_x linear algebraic equations in the J_x unknowns $I^{n,x}_j$. The system is tridiagonal and is solved by a simple elimination scheme. As stated above, the R_x operator makes no change in densities or velocities.

B. EQUATION FOR RADIATION LOSS

In calculating D_{rad}, the loss rate per unit mass of thermal radiation (Eq. 10), we evaluate the angular integral by a sum over four directions:

$$D_{rad} \approx j_4(\rho,T) \left[\exp\left(-\tau(\hat{r})\right) + \exp\left(-\tau(-\hat{r})\right) + \exp\left(-\tau(\hat{z})\right) + \exp\left(-\tau(-\hat{z})\right)\right] \Delta\Omega,$$

where $\Delta\Omega = \pi$ sterad. This form makes it convenient to split D_{rad}

and include the first two terms in the R_r operator and the last two in the R_z operator. We denote the two parts by D_r and D_z, so that

$$D_{rad} = D_r + D_z. \tag{24}$$

We can then use the abbreviated (single-subscript) notation of the previous subsection, in which x denotes r or z and only the subscript referring to the x direction is retained.

In evaluating $\tau(\hat{x})$ for a given cell, we use Eq. (9) and assume that ρ and I are constant throughout each cell. The optical thickness (for 0 to 4.13 ev photons) of cell j along a direction $\hat{x}$ is

$$\Delta\tau_j^n(\hat{x}) \equiv \kappa_{p4}(\rho_j^n, T_j^n)\ \rho_j^n\ \Delta x_j \qquad \text{for } 1 \le j \le J_x, \tag{25}$$

and the optical depth from the right (or top) edge of cell j to the right (or top) boundary of the problem in the $\hat{x}$ direction is

$$\tau_{j+1/2}^n(\hat{x}) \equiv \sum_{i=j+1}^{J_x} \Delta\tau_i^n(\hat{x}) \qquad \text{for } 0 \le j \le J_x - 1, \tag{26}$$

and that from the left (or bottom) edge of cell j to the left (or bottom) boundary of the problem in the $-\hat{x}$ direction is

$$\tau_{j-1/2}^n(-\hat{x}) \equiv \begin{cases} \displaystyle\sum_{i=1}^{j-1} \Delta\tau_i^n(\hat{r}) + \sum_{i=1}^{J_r} \Delta\tau_i^n(\hat{r}) & \text{if } x = r, \\ \displaystyle\sum_{i=1}^{j-1} \Delta\tau_i^n(\hat{z}) & \text{if } x = z. \end{cases} \tag{27}$$

Because of the coarseness of our grid, some cells that radiate strongly are optically thick ($\Delta\tau_j^n \gtrsim 1$). In order to account reasonably for the self-absorption within a cell we allow $\tau(\hat{x})$ and $\tau(-\hat{x})$ to vary through the cell,

$$\tau(\hat{x}) = \kappa_{P4}(\rho_j^n, T_j^n)\, \rho_j^n \left(x_{j+1/2} - x\right) + \tau_{j+1/2}^n (\hat{x}) \tag{28}$$

and similarly for $\tau(-\hat{x})$, and average D_{rad} over the mass of each cell. Thus, the part of D_{rad} that is included in the R_x operation is

$$(D_x)_j^n \equiv \frac{c_R \int_{cell\ j} j_4(\rho,T) \left\{\exp\left[-\tau(\hat{x})\right] + \exp\left[-\tau(-\hat{x})\right]\right\} \Delta\Omega\, \rho\ dV}{\int_{cell\ j} \rho\ dV};$$

here c_R is a calibration constant discussed in Sec. III-D. We assume that ρ and $j_4(\rho,T)$ are constant throughout the cell, and we ignore any variation through the cell of its cross-sectional area perpendicular to the x direction. An integral useful in evaluating the above equation is

$$\frac{1}{\Delta x_j} \int_{x_{j-1/2}}^{x_{j+1/2}} \exp\left[-\tau(\hat{x})\right] dx = \exp\left[-\tau_{j+1/2}^n (\hat{x})\right] \frac{\left\{1-\exp\left[-\Delta\tau_j^n(\hat{x})\right]\right\}}{\Delta\tau_j^n(\hat{x})},$$

and the final result for $(D_x)_j^n$ is

$$\begin{aligned}(D_x)_j^n = c_R \kappa_{P4}(\rho_j^n, T_j^n) f_4(T_j^n)\, \frac{\sigma\left[T_j^n\right]^4}{\pi} \left\{\exp\left[-\tau_{j+1/2}^n (\hat{x})\right] + \exp\left[-\tau_{j-1/2}^n (-\hat{x})\right]\right\} \\ \times \left\{\frac{1-\exp\left[-\Delta\tau_j^n(\hat{x})\right]}{\Delta\tau_j^n(\hat{x})}\right\} \Delta\Omega\,.\end{aligned} \tag{29}$$

A simpler calculation (setting $x=x_j$ in Eq. 28) would have given $\exp[-0.5\Delta\tau_j^n(\hat{x})]$ in place of the expression in large braces; for optically thin cells ($\Delta\tau_j^n(\hat{x})<<1$) these expressions are equal, but when one cell is optically thick and those in front of it are optically thin, only Eq.(29) reduces correctly to blackbody radiation from the surface of the cell.

C. CHOICE OF TIME STEP AND SPATIAL GRID

An implicit difference scheme, such as used here to treat radiation, is numerically stable with much larger time steps than an explicit scheme. The present scheme for radiation diffusion is stable enough so that accuracy, rather than numerical stability, limits the size of time step. We limit the time step by requiring that the change in specific internal energy of each cell during each operation (R_r and R_z) must not exceed a given fraction c_{rad} (we use $c_{rad} = 0.025$) of the maximum specific internal energy anywhere at that time:

$$\Delta t_{rad}^{n+1/2} \equiv \frac{c_{rad} \max\limits_{k,\ell} \left(I_{k,\ell}^{n-1,x} \right)}{\max\limits_{k,\ell,x} \left(I_{k,\ell}^{n-1,x} - I_{k,\ell}^{n-1} \right) \Big/ \Delta t^{n-1/2}} \quad . \tag{30}$$

At later times numerical stability of the hydrodynamics also limits the time step (Ref. 1, pg. 2):

$$\Delta t_{hyd}^{n+1/2} \equiv c_{hyd} \min_{k,\ell,x} \left(\frac{\Delta x_{k,\ell}}{(v_x)_{k,\ell}^{n-1,x}} \right), \tag{31}$$

with

$$\Delta t^{n+1/2} = \min \left(\Delta t_{rad}^{n+1/2} , \Delta t_{hyd}^{n+1/2} \right). \tag{32}$$

We find $c_{hyd} = 0.2$ satisfactory.

The spatial grid is chosen to have a finely gridded region of 21 x 41 cells around each burst during its growth stage. (When a second burst occurs, the finely gridded region is achieved by having a vertical strip of narrow cells intersect a horizontal strip of short cells.) The size of these square cells is chosen so that the initial fireball radius is at least 8 cells long. The time at which the fireball radius will expand to 16 cells is then estimated by means of an empirical dimensionless curve of fireball radius vs. time. At that time we convert all variables to a new grid, having cells in the fireball region that are twice as large in each direction. This process is repeated as needed.

The outer part of the grid is nonuniform, each cell being 20 per cent longer or wider than its inner neighbor. Shock waves are allowed to run off the edge of the grid when they become moderate to weak.

The artificial diffusion has the same form as in Ref. 1, Eq. (42); the coefficients q_1, q_2, q_3, and q_4 are chosen to be 0.5 while the shock is strong and to be 0.03 at late time. The artificial viscous pressure Q (Ref. 1, Section III) is unchanged in form; its coefficient q_{22} is chosen to be 1.0.

D. CALIBRATION OF RADIATION LOSS

Predicting the total radiation loss for low-altitude bursts is especially important, for the late-time hydrodynamics depends on the amount of energy remaining in the burst region. We checked the radiation loss predicted by our method (with calibration factor $c_R = 1.0$ in Eq. 29) against that predicted by the RADFLO code. Using a one-dimensional spatial grid, the agreement is satisfactory. (The power vs. time curves generally peak somewhat too early and too high).

Using the two-dimensional grid required for interacting-fireball calculations results in radiation loss predictions that are too low. The coarser cells necessary in a two-dimensional calculation seem mainly responsible for this error. To correct for this we increase the radiation loss rate (Eq. 29) by a calibration factor c_R. The predicted radiation loss for an event of small yield is satisfactory if $c_R = 2.5$ when the grid is two-dimensional and $c_R = 1.0$ when it is one-dimensional.

IV CONCLUSION

The code has been used to calculate a series of nine problems involving two identical bursts separated in space and time. The results will be reported elsewhere by Christian, Stoeckly, and Schlueter.

On a CDC 7600 computer using the RUN compiler, computation time is about 1 millisec per cell per time step for hydrodynamics and 0.5 millisec per cell per time step for radiation diffusion. After 2 sec of problem time the radiation diffusion terms are dropped from the calculations. Total computation time for a problem of two close bursts over the time interval $0 < t < 120$ sec (2000 cycles) using a coarse spatial grid averaging 20×40 cells is 40 min on a CDC 7600.

REFERENCES

1. Fajen, F. E., MICE: An Implicit Difference Scheme for MHD Calculations, DNA-2877Z, MRC-R-12, Mission Research Corporation, March 1973.

2. Allen, C. W., Astrophysical Quantities, second edition, University of London (1963), Sec. 43, p. 103.

3. Hilsenrath, J., M. G. Green, and C. W. Beckett, Thermodynamic Properties of Highly Ionized Air, SWC-TR-56-35, Air Force Special Weapons Center, April 1957.

4. Hilsenrath, J., M. Klein, and H. W. Woolley, Tables of Thermodynamic Properties of Air Including Dissociation and Ionization From 1500° K to 15000° K, AEDC-TR-59-20, National Bureau of Standards, December 1959.

5. Gilmore, F. R., Equilibrium Composition and Thermodynamic Properties of Air to 24000° K, RM-1543, The Rand Corporation, August 1955.

6. Brode, H. L., W. Asano, M. Plemmons, L. Scantlin, and A. Stevenson, A Program for Calculating Radiation Flow and Hydrodynamic Motion, RM-5187-PR, The Rand Corporation, April 1967, pp. 75, 64, and 293.

7. Sowle, D. H., P. G. Fischer, and D. S. Sappenfield, An All-Altitude Air Burst Code. Vol. I: New Techniques, MRC-R-21, Mission Research Corporation, July 1972.

8. U. S. Standard Atmosphere, 1962, U. S. Government Printing Office, December 1962.

9. McMaster, W. H., and others, Compilation of X-ray Cross Sections, UCRL-50174, Lawrence Radiation Laboratory, January 1967, Section II.

10. Huffman, R. E., "Photochemical Processes: Cross-Section Data," Chapter 12 in Defense Nuclear Agency Reaction Rate Handbook, Second Edition, DNA 1948H, edited by M. H. Bortner and T. Baurer, General Electric TEMPO, Santa Barbara, 1972. See Fig. 12-10 and Ref. 12-48.

THIS PAGE INTENTIONALLY LEFT BLANK.

DISTRIBUTION LIST

DEPARTMENT OF DEFENSE

Defense Documentation Center
12 cy ATTN: TC

Director
Defense Nuclear Agency
ATTN: STSI, Archives
ATTN: DDST
2 cy ATTN: STTL, Tech. Library
3 cy ATTN: RAAE

Director of Defense Research & Engineering
ATTN: OAD/EPS, Lieutenant Colonel W. A. Whitaker

Commander
Field Command
Defense Nuclear Agency
ATTN: FCPR

Chief
Livermore Division, Field Command, DNA
Lawrence Livermore Laboratory
ATTN: FCPRL

OJCS/J-3
The Pentagon
ATTN: J-3, Ops. Anal. Br., Colonel Underhill

Weapons Systems Evaluation Group
ATTN: Document Control

DEPARTMENT OF THE ARMY

Commander
Ballistic Defense System Command
2 cy ATTN: SSC-HS, H. Porter

Director
Ballistic Missile Defense Advanced Tech Center
ATTN: CRDABH-O, W. Davies

Manager Ballistic Defense Program Office
ATTN: DACS-BMS, Julian Davidson
ATTN: John Shea
ATTN: CRDABM-RP

Commander
Harry Diamond Laboratories
ATTN: AMXDO-NP
ATTN: AMXDO-NP, Dr. Wimenitz

Commander
TRASANA
ATTN: R. E. DeKinder, Jr.

Director
U.S. Army Ballistic Research Laboratories
ATTN: AMXBR-CA, Franklin E. Niles

Commander
U.S. Army Material Command
ATTN: P. Crowley

Commander
U.S. Army Materiel Command
ATTN: AMCRD-WN-RE, John F. Corrigan

DEPARTMENT OF THE ARMY (Continued)

Commander
U.S. Army Nuclear Agency
ATTN: USANUA-W, J. Berberet

DEPARTMENT OF THE NAVY

Chief of Naval Research
Department of the Navy
ATTN: Code 418, Gracen R. Joiner

Director
Naval Research Laboratory
ATTN: Code 7750, Timothy P. Coffey
ATTN: Code 7701, Jack D. Brown

Commander
Naval Surface Weapons Center
ATTN: Code 1224, Navy Nuc. Prgms. Off.

DEPARTMENT OF THE AIR FORCE

ADC/XP
ATTN: XPDW, Maj Kuch

AF Cambridge Research Laboratories, AFSC
ATTN: OPR, Alva T. Stair
ATTN: LKB, Kenneth S. W. Champion

AF Weapons Laboratory
ATTN: CA, Fol Frier
ATTN: DYT, Capt Daniel A. Matuska
ATTN: SUL

AFTAC
ATTN: TAP, Maj E. Hines

Commander
Rome Air Development Center
ATTN: EMTLD, Document Library

HQ USAF/RD
ATTN: RDQ

ENERGY RESEARCH & DEVELOPMENT ADMINISTRATION

Los Alamos Scientific Laboratory
ATTN: Document Control for Eric Jones
ATTN: Document Control for Herman Hoerlin

Sandia Laboratories
ATTN: Document Control for D. A. Dahlgren

DEPARTMENT OF DEFENSE CONTRACTORS

Aeronautical Research Association of Princeton, Inc.
ATTN: Coleman Donaldson

Aerospace Corporation
ATTN: V. Josephson

Brown Engineering Company, Inc.
2 cy ATTN: David Lambert
2 cy ATTN: C. Wayne

DEPARTMENT OF DEFENSE CONTRACTORS (Continued)

Calspan Corporation
ATTN: Romeo A. Deliberis

Computer Sciences Corporation
Huntsville Operations
ATTN: Joe Parrott

General Electric Company
TEMPO-Center for Advanced Studies
ATTN: DASIAC
ATTN: T. Barrett
ATTN: Ed Martin
ATTN: Warren S. Knapp

General Research Corporation
ATTN: John Boys
ATTN: John Ise, Jr.

HSS, Inc.
ATTN: Donald Hansen

Information Science, Inc.
ATTN: Walter F. Dudziak

Institute for Defense Analyses
ATTN: Ernest Bauer

Lockheed Missiles & Space Company
ATTN: Roland E. Meyerott

Martin Marietta Aerospace
Orlando Division
ATTN: Roy W. Heffner

McDonnell Douglas Corporation
ATTN: Robert W. Halprin

Mission Research Corporation
ATTN: Dave Sowle
ATTN: Gary McCarter
ATTN: P. Fischer
ATTN: Robert E. Stoeckly
5 cy ATTN: Document Control

DEPARTMENT OF DEFENSE CONTRACTORS (Continued)

Mount Auburn Research Associates, Inc.
ATTN: Sheldon L. Kahalas

Photometrics, Inc.
ATTN: Irving L. Kofsky

Physical Dynamics, Inc.
ATTN: A. Thompson

R & D Associates
ATTN: Forest Gilmore
ATTN: Robert E. Lelevier

The Rand Corporation
ATTN: Cullen Crain

Science Applications, Inc.
ATTN: William M. Layson

Science Applications, Inc.
ATTN: D. Sachs
ATTN: Jim Young

Stanford Research Institute
ATTN: L. L. Cobb
ATTN: Walter G. Chestnut

Technology International Corporation
ATTN: W. P. Boquist

TRW Systems Group
ATTN: J. Chang